JKAU: Eng. Sci., **Vol. 16** No. 2, pp: 117-136 (2005 A.D. / 1426 A.H.)

Natural Convection in a Tilted Rectangular Enclosure with a Single Discrete Heater

A. Al-Bahi*, M. Al-Hazmy and G. M. Zaki

**Aeronautical Engineering Department and Mechanical Engineering Department, Faculty of Engineering College of Engineering, King Abdulaziz University P. O. Box 80204, Jeddah 21589, Saudi Arabia*

Abstract. The effect of inclination angle on the steady laminar free convection in a rectangular enclosure (aspect ratio = 5), which is discretely heated by an isoflux flush mounted small heater (L / H = 0.125) is studied numerically. The local and average Nusselt numbers are compared at inclination angles from 0 (bottom heating) to 180º (top heating), for modified Rayleigh numbers $10^2 \leq Ra^* \leq 10^6$. The two-dimensional mass, momentum and energy equations with Boussinesq approximation are solved for the present configuration where the sidewalls are adiabatic and the heat sink is isothermal. Forward time central space implicit finite difference scheme is employed to solve the coupled governing equations. Numerical results demonstrate the strong dependence of streamlines and isotherms on both inclination angle and Rayleigh number. Unlike fully heated enclosures the end effects of the discrete concentrated heat source enhances convection and increases the average Nusselt number as compared to that for thermally full active wall. The effect of the orientation angle on the flow structure and associated transition between unicellular and multiple cell flow is presented. The maximum Nusselt number is found close to the vertical orientation while the minimum is at the horizontal position with fluid heated from the top for which convection is effectual and the average Nusselt number is greater than unity.

Keywords: Natural convection, enclosure, discrete heater, Nusselt number.

*Corresponding author: *dr_bahi@yahoo.com*

1. Introduction

Natural convection in enclosures is encountered in many engineering systems. Convection in buildings, heat transfer in solar systems, cooling of electronic circuits, and coolability of nuclear fuel under accident scenario are examples of these applications, where free convection is the dominating heat transport mechanism. The principal advantage of free convection is the reliability, where convection currents are naturally generated without the need to prime movers as pumps or fans.

The review papers by Catton[1], Yang[2], Ostrach[3] and Khalifa[4] reveal the importance of convection in enclosures. Representative studies on differentially heated enclosures may be categorized as *full contact* vertical[5-9] and tilted[10-21] enclosures, for which the buoyancy is created by the thermal gradient between a full size heat source on one wall and an equal size cold sink on the opposite wall. Raithby and Holland[17] have presented the fundamentals of free convection within enclosures of full contact heated walls. Cooling of integrated circuits and microelectronic chips drew attention to enclosures with concentrated heat sources, namely, *discretely heated* enclosures, which are comprehensively reviewed by Incropera[22], Sathe and Samakia[23] and Teertstra[24]. Several other studies on natural convection from discrete heaters covered different heating conditions, aspect ratio and inclination angle[25-33].

The studies of Chu *et al.*[25] and Refai and Yovanovich[26-27] are basic contributions, where Nusselt number in vertical enclosures with a single heat source was computed. Research in this area was extended to include single isoflux, Chadwick *et al.*[28], and dual isothermal, Turner and Flack[29], discrete heaters. Ho and Chang[30] and Keyhani *et al.*[31] obtained correlations for multiple isoflux discrete heaters in rectangular enclosures. Radhwan and Zaki[32] and Al-Bahi *et al.*[33] studied the effect of heater's location on the heat transfer and flow field in a vertical square enclosure. Silva *et al.*[34] investigated the optimum positioning of a number of discrete heat sources cooled by laminar convection in an enclosure for randomly distributed small heaters and finite-size heat sources. Deng *et al.*[35] investigated the case of a square enclosure with heat sources on two sides and a single heat sink. Tou and Zhang[36] considered the case of a tilted enclosure with an array of discrete heaters; reporting that the average Nusselt number for an array of heaters compared well with the empirical correlations obtained for a single heater. Sezai and Mohamad[37] studied an enclosure with a discrete heater on the horizontal wall. They related Nusselt number to Rayleigh number and the aspect ratio of the heat source

It is evident that a substantial amount of work is available for fully heated vertical and tilted enclosures as well as discretely heated vertical enclosure. There is lack of fundamental information regarding the flow structure and heat

transfer in inclined discretely heated enclosures. This study covers the entire range of tilt angles and the effects of Rayleigh number on the flow and heat transfer characteristics in a rectangular enclosure (aspect ratio = 5) with a single isoflux discrete heat source. The inclination angle varied from 0 to 180º ($0 \leq \varphi \leq \pi$) presenting a cavity with bottom heating (in analogy to Rayleigh-Benard problem) and heat-ing from the top respectively.

2. Mathematical Formulation

The geometry of interest for this study is shown in Fig. 1. The study is limited to two dimensional flow in a rectangular cavity of length H and width W. A discrete isoflux heating strip of length L is flush-mounted to the wall at $x = 0$ and a distance s measured to the center of the heater. The opposite wall ($x = W$) is an isothermal heat sink at T_c. All other surfaces, $y = 0$, $y = H$, $s + L/2 < y < H$ and $0 < y < s\text{-}L/2$ are insulated. The enclosure is tilted at an angle φ measured between the horizontal direction and the heating surface, such that $\varphi = 90º$ presents a vertical enclosure and $\varphi = 180º$ is a situation for a cavity heated from the top.

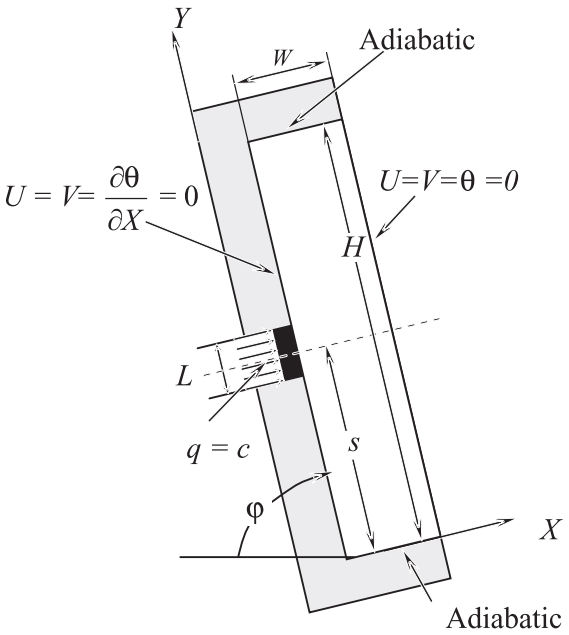

Fig. 1. Schematic of the enclosure configurations.

The cavity is filled with an incompressible Newtonian fluid and the Boussinesq approximations are assumed. The dimensionless governing mass, momentum and energy equations are as follows, from Nogotov[38]:

Continuity

$$\frac{\partial U}{\partial X}+\frac{\partial V}{\partial Y}=0 \tag{1}$$

x direction momentum

$$\frac{\partial U}{\partial \tau}+U\frac{\partial U}{\partial X}=V\frac{\partial U}{\partial Y}=-\frac{\partial P}{\partial X}+\frac{1}{\mathrm{Re}}\nabla^2 U+\frac{Ra*}{\mathrm{PR}\,\mathrm{Re}^2}\theta\ \ \mathrm{Cos}\ \varphi \tag{2}$$

y direction momentum

$$\frac{\partial V}{\partial \tau}+U\frac{\partial V}{\partial X}=V\frac{\partial V}{\partial Y}=-\frac{\partial P}{\partial Y}+\frac{1}{\mathrm{Re}}\nabla^2 V+\frac{Ra*}{\mathrm{PR}\,\mathrm{Re}^2}\theta\ \ \mathrm{Sin}\ \varphi \tag{3}$$

Energy equation

$$\frac{\partial \theta}{\partial \tau}+U\frac{\partial \theta}{\partial X}=V\frac{\partial \theta}{\partial Y}=\frac{1}{\mathrm{Re}\,\mathrm{PR}}\nabla^2\theta \tag{4}$$

The dimensionless variables used in Eq. 1-4 are:

$X = x/W$ $\qquad$ $Y = y/W$

$U = u/v_0$ $\qquad$ $V = v/v_0$

$\theta = (T\text{-}T_c) / (qW/k)$

$Ra^* = Gr^*\ Pr = g\beta qW^4 / k\upsilon\alpha$

$Re = v_o W/\upsilon$ $\qquad$ and $\qquad$ $\tau = tv_0/W = t/t_0$

The system of Eq. 1-4 describes a general convection condition for which is Gr^* / Re^2 the governing parameter. For free convection the Reynolds number becomes unity as the reference velocity v_o is assumed to be υ/W, and for this condition the reference time is $t_0 = W^2/\upsilon$.

Eliminating the pressure between Eq. 2 and 3 by cross differentiation and subtraction and introducing a dimensionless stream function ψ, and vorticity, ω Eq. 1-4 become:

$$\frac{\partial^2 \psi}{\partial X^2}+\frac{\partial^2 \psi}{\partial^2 Y^2}=-\omega \tag{5}$$

$$\frac{\partial \omega}{\partial \tau}+U\frac{\partial \omega}{\partial X}+V\frac{\partial \omega}{\partial Y}=\frac{\partial^2 \omega}{\partial X^2}+\frac{\partial^2 \omega}{\partial Y^2}+\mathrm{G\,r}^*\left[\frac{\partial \theta}{\partial X}\mathrm{Sin}\,\varphi-\frac{\partial \theta}{\partial Y}\mathrm{Cos}\,\varphi\right] \tag{6}$$

$$\frac{\partial\theta}{\partial\tau}+U\frac{\partial\theta}{\partial X}+V\frac{\partial\theta}{\partial Y}=\frac{1}{\mathrm{Pr}}\left[\frac{\partial^2\theta}{\partial X^2}+\frac{\partial^2\theta}{\partial Y^2}\right] \tag{7}$$

where $U=\dfrac{\partial\psi}{\partial Y}$ and $V=-\dfrac{\partial\psi}{\partial X}$

The initial and boundary conditions, Fig. 1, are:

Initial condition

$$\begin{aligned}&\text{at } \tau=0, \quad 0\le X\le 1, \quad 0\le Y\le L/W\\ &\psi=\theta=0\end{aligned} \tag{8}$$

Boundary conditions at X = 0

$$\begin{aligned}&\text{at } \tau>0, \quad X=0 \quad 0\le Y\le L/W\\ &\psi=0, \quad \frac{\partial\psi}{\partial X}=0,\end{aligned} \tag{9}$$

$$\frac{\partial\theta}{\partial X}=-1 \qquad (s-L/2)/W\le Y\le (s+L/2)/W \tag{10}$$

$$\frac{\partial\theta}{\partial X}=0 \qquad 0<Y<(s-L/2)/W \text{ and } (s+L/2)/W<Y<H/W \tag{11}$$

Boundary conditions at X = 1

$$\begin{aligned}&\tau>0, \quad X=1 \quad 0\le Y\le L/W\\ &\psi=0, \quad \theta=\frac{\partial\psi}{\partial X}=0\end{aligned} \tag{12}$$

Boundary at X = 0

$$\begin{aligned}&\tau>0, \quad Y=0 \quad 0<X<1\\ &\psi=0, \quad \frac{\partial\psi}{\partial Y}=0, \quad \frac{\partial\theta}{\partial Y}=0\end{aligned} \tag{13}$$

Boundary at Y = L/W

$$\begin{aligned}&\tau>0, \quad 0\le X\le 1\\ &\psi=0, \quad \frac{\partial\psi}{\partial Y}=0, \quad \frac{\partial\theta}{\partial Y}=0\end{aligned} \tag{14}$$

The modified Rayleigh number *Ra** and Nusselt number are based on the width of the enclosure *W*, which gives a physical meaning for the dimensionless temperature, θ, as the ratio between the temperature gradient with convection to that with pure conduction across the width. The position of the heater is determined by $\varepsilon = s/H$ and the size of the heater length to enclosure height is $\gamma = L / H$. Full contact heater, where one wall is fully heated is characterized by $\varepsilon = 0.5$ and $\gamma = 1$. The local heat transfer rate at the hot section is presented by the local Nusselt number, *Nu* and the averaged Nusselt number, $\overline{Nu}$ are defined for isoflux condition as:

$$Nu = \frac{qW}{k(T_s - T_c)} = \frac{1}{\theta}\bigg|_{X=0} \qquad Y_1 \le Y \le Y_2 \tag{15}$$

and

$$\overline{Nu} = qW / k\overline{(T - T_c)} \; = qWL / k \int_0^L (T - T_c)dy = 1/\overline{\theta_s} \tag{16}$$

where,

$$Y_1 = \frac{s - L/2}{W} \quad \text{and} \quad Y_2 = \frac{s + L/2}{W}$$

Local Nusselt number at the isothermal cold wall is;

$$Nu_c = -\frac{\partial\theta}{\partial X}\bigg|_{X=1} \qquad 0 \le Y \le H/W \tag{17}$$

3. Solution Procedure

Equations 5 through 7 are solved using a forward in time and centered in space finite difference approach, which follows a stabilizing correction splitting, alternate direction implicit (ADI) scheme[39]. The governing equations were discretized using second order difference approximation on a nonuniform grid. The mesh is refined near the longer walls to account for the thermal and hydraulic boundary layers. Central difference relations were used for the diffusion terms, Eq. 5, while the convective terms, Eq. 6, were treated by a second order upwind difference scheme (Shyy *et al.*[40]). On all boundaries, no slip conditions were imposed. In order to solve the vorticity equation near the walls a second order difference approximation of ψ was used. For this approximation ψ outside the computational domain (image points) were calculated by a Taylor second order expansion. This technique relates the boundary condition for

vorticity to stream function only. For example, the expression of ω at the surface ($x = 0$, $i = 1$ and $\omega_{1,j} = \omega(x = 0, j\Delta y)$) in difference form is: with non-uniform grid with;

$$\omega_{1,j} = -\frac{\psi_{1,j+1} - 2\psi_{1,i} + \psi_{1,j-1}}{2(\Delta x)^2} \tag{18}$$

The last term of the nominator is the value at an image point obtained for a nonuniform mesh (the nodes vary in size according to $\alpha = \Delta x_{1,j+1} / \Delta_{x1,j}$) as,

$$\psi_{1,j-1} = -\frac{2(\alpha+2)}{(1+\alpha)^2}\psi_{1,j} + \frac{(2+\alpha)}{2}\psi_{1,j+1} - \frac{2}{\alpha(1+\alpha)^2}\psi_{1,j+2} \tag{19}$$

For a uniform grid $\alpha = 1$ this leads to the condition of Koskova, recommended by Nogotov[38].

The steady state solution was obtained as the limit of the transient calculations. The solution routine starts by assuming initial values for all variables, then the stream function equation was iteratively satisfied for every time step. Five to ten iterations were found to be sufficient, for a dimensionless time step of 5×10^{-4}. The convergence criteria was examined for every variable (ψ, ω and θ) employing the normalized residue R such that;

$$R = \frac{\max\left|\lambda_{ij}^{n} - \lambda_{i,j}^{n+1}\right|}{\max\left|\lambda_{ij}^{n+1}\right|} \leq \xi_{\lambda} \tag{20}$$

where n is the iteration level, λ_{ij} is any of the variables (ψ, ω and θ), ξ_{λ} is the accuracy limit set to $2.\ 10^{-8}$ for $Ra^* = 10^6$ and nonuniform 100×25 grid.

4. Solution Verification

The developed solution algorithm has been validated by performing calculations for the standard square enclosure problem with two isothermal walls ($\varepsilon = 1$ and $s/H = 0.5$, Aspect ratio $Ar = 1$) and compare the results with the benchmark solutions of De-Vahl Davis[5]. The results were found to be in good agreement with the corresponding results as seen in Table 1. The percentage deviation between the present algorithm and the benchmark solution D% is obtained for different parameters and grid sizes, (Table 1). The maximum deviation in $\overline{Nu}$ is less than 1% for mesh size greater than 80×80. The stretched grid showed better performance where the deviation in all parameters is less than 1%, in particular 0.089% for average Nusselt number and 51×51 stretched grid. These results verify the present solution algorithm. Further validation was carried out

for the configuration and boundary conditions of Chadwick[28] (rectangular enclosure $Ar = 5$ with an isoflux discrete flush heater $\varepsilon = 0.133$ and $s/L = 0.5$) Grashof number of 5.16×10^5. For this comparison a nonuniform stretched 51×51 grid was used and the results for streamlines and isotherms are in good agreement with the published results (Fig. 2).

Table 1. Comparison of present algorithm with the Benchmark[5] solution at $Ra = 105$.

Grid	De Vahl Davis[5]	Uniform grid				Stretched grid	
		81 × 81	121 × 121	16 × 161	181 × 181	51 × 51	101 × 101
Nu_{max} D%	7.717 –	7.848 (1.697)	7.787 (0.907)	7.763 (0.596)	7.756 (0.505)	7.77 (0.687)	7.741 (0.311)
Nu_{min} D%	0.729 –	.721 (1.097)	0.724 (0.686)	0.726 (0.413)	0.726 (0.413)	0.723 (0.823)	0.727 (0.274)
$\overline{Nu}$ D%	4.509 –	4.504 (1.109)	4.513 (0.887)	4.515 (0.133)	4.515 (0.133)	4.505 (0.089)	4.514 (0.111)

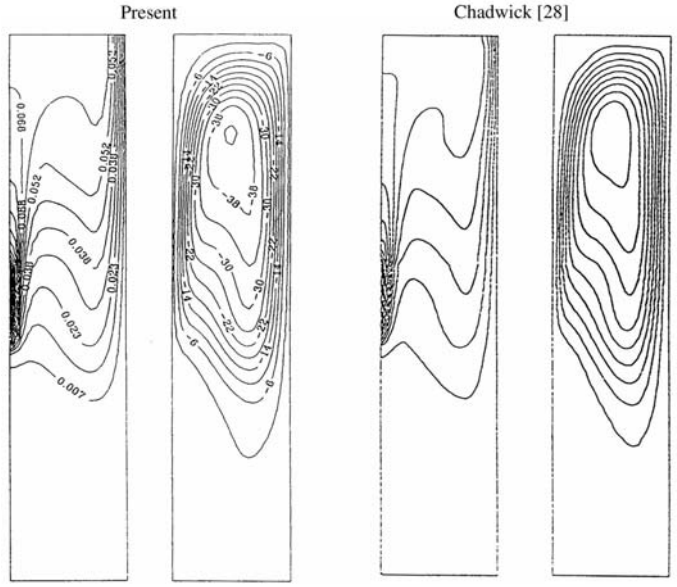

Fig. 2. Verification of the present solution as compared to that of Chadwick[28], $H/W = 5$, $L/H = 0.13$ and $Gr = 5.16 \times 10^5$.

Grid dependence was examined by computing $\overline{Nu}$ for a series of nonuniform grids and comparing the values. Test runs were performed for stretched grids from 50×25 to 240×50 mesh size at $Ra^* = 10^5$, $\varphi = 45$ and 90º. Assuming the average Nusselt number for 240×50 grid is a reference value, the results showed that the maximum deviation of –1.2% was obtained at $Ra^* = 10^5$, 90º tilt angle and 50×50 stretched grid.

Table 2 shows that the deviation for any other grid selection is acceptable. As a trade off between computation time and accuracy 100×25 stretched grid was used for the remaining computation.

Table 2. Dependency of $\overline{Nu}$ on grid size at $Ra^* = 10^5$.

Grid size	Deviation % in $\overline{Nu}$	
	$\varphi = 90^o$	$\varphi = 45^o$
50×25	(0.70)	(–0.95)
50×50	(–1.25)	(–1.20)
100×25	(0.14)	(0.00)
100×50	(–0.47)	(–0.51)
100×100	(–0.51)	(–0.43)

5. Results and Discussion

For the present work the effect of two parameters, the tilt angle and Rayleigh number, on natural convection in a rectangular enclosure are investigated. Other parameters are fixed at $\gamma = 0.125$, $s/H = 0.5$ and $Pr = 1$.

5.1 Streamlines and Isotherms

Interesting features for the tilted enclosures are associated to the variations of streamlines and isotherms with the tilt angle. The computed flow fields for tilt angles between 0 and 180º are presented in Fig. 3. The corresponding isotherms for $Ra^* = 10^6$ are shown in Fig. 4.

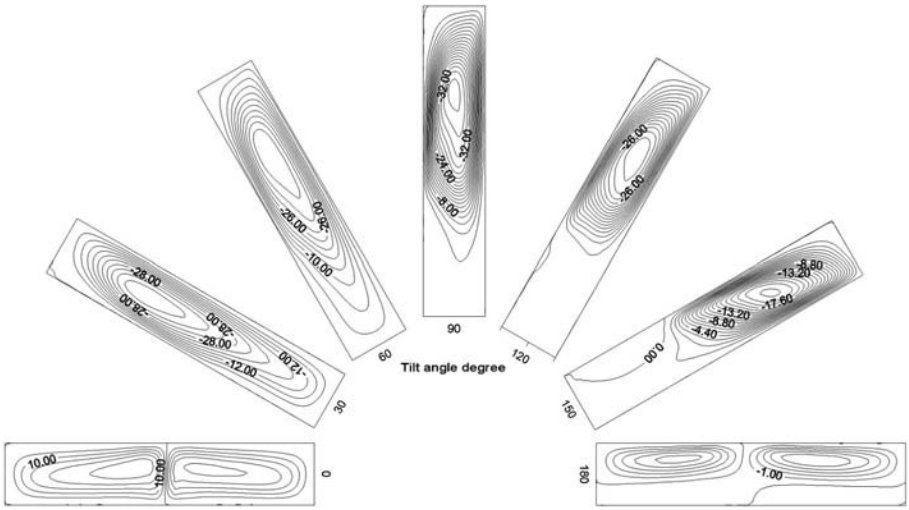

Fig. 3. Streamlines for discretely heated enclosure at $Ra^*=10^6$.

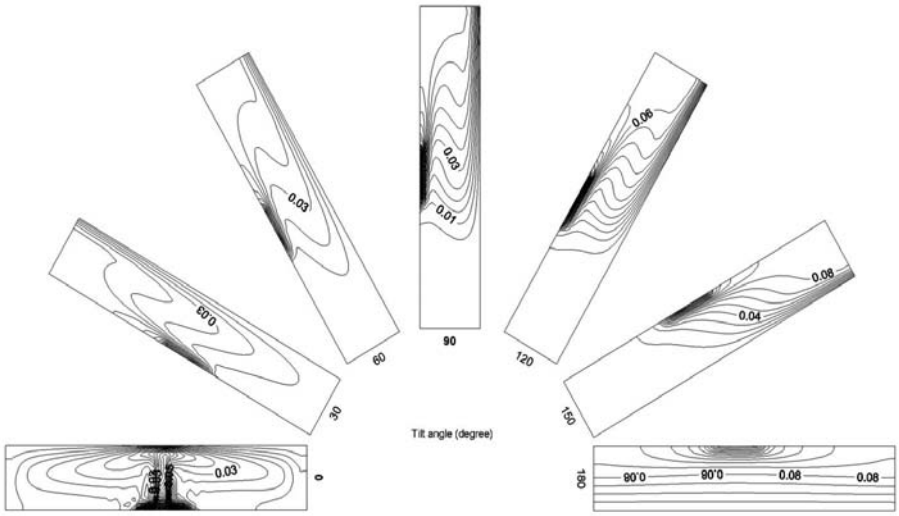

Fig. 4. Variation of isotherms with tilt angle, $Ra^*=10^6$.

At the horizontal orientation, φ = 0º the streamlines form two cells with opposite rotational directions and have a maximum stream function $|\psi_{max}|$ = 28.35. This flow structure is created when the rising hot fluid reaches the cold surface and returns along the adiabatic walls forming two stretched cells. The corresponding isotherms form a mushroom pattern as depicted in Fig. 4. The shown structure is entirely different from that for a full heating, ε = 1 where Benard cells are formed at a size nearly equal to the cavity width.

For inclination angles of 30º up to 60º and Ra^* = 10^6 convection is evident and a single enlarged cell characterizes the flow. The flow transition from a two cells pattern to unicellular occurs at an angle between 15 and 22º where the numerical solution did not converge even with grid refinement. This unstable region was not considered where the two-dimensional model might not be sufficient to describe the transition. Kuyper *et al.*[20] reported on a transition angle for a tilted square enclosure in the same order. The shown streamlines and isotherms for these angles suggest a boundary layer type flow along both the discrete heater section and the upper part of the cold wall where isotherms are clustered along these sections. The maximum value of the stream function is nearly constant within this range $|\psi_{max}|$ = 43.01 at φ = 30º and $|\psi_{max}|$ = 41.91 at φ = 60º).

At the vertical position where the gravitational field is parallel to the boundary layer the circulation cell is squeezed towards the upper section of the enclosure (Fig. 3). The isotherms show that convection is still confined along the short discrete heater and a short length of the cold wall. For further increase

in tilt angle to 120 and 150º the flow maintains unicellular pattern with the tendency to decrease the rotational velocity with the tilt angle ($|\psi_{max}|$ = 33 at 120º and drops to 21 at 150º) as seen in Fig. 3. This trend decreases the heat transfer rate as the enclosure approaches the top heating horizontal position, φ = 180º. At this orientation, the isotherms flatten to become horizontal (Fig. 4) indicating conduction dominated heat transfer across the lower part of the cavity. An interesting result shown here is the presence of weak convection at this top heating position, which is not the case for fully heated enclosures presented by Elsherbiny[16&21] and Ozoe[15] for rectangular and square cavities respectively. The case for fully heated enclosure with the present aspect ratio, A_r = 5 and isoflux heater was computed and the results showed established stratified fluid domain with pure conduction heat transfer mode across the whole cavity. The computed average Nusselt number varied between 1 and 1.037 at, Ra^* = 10^3 and 10^6 respectively. For discrete heaters probably the end effects of the heater cause enhancement of the heat transfer rate and flow circulation develops forming two roll cells within the upper section of the cavity with weak strength, where $|\psi_{max}|$ = 5, as seen in Fig. 3 at φ = 180º.

5.2 Nusselt Number

Figure 5 shows the local Nusselt number variation along the heater length for Ra^* = 10^3 to 10^6 and inclination angles from 0 to 180º. At φ = 0º, the symmetrical variation *Nu* of indicated high heat transfer at both ends of the heater with minimum at the center due to the presence of a stagnation flow condition. Nusselt number variation is well explained by the flow structure shown in Fig. 3 where two separate rotational cells are formed at Ra^* = 10^6. Consequently, Nusselt number variation is different from that for the case of fully heated enclosure where Nusselt number varies in a wavy pattern[17]. The fully heated horizontal bottom-heating cavity develops a flow structure and heat transfer feature as if it is made of segments of adjacent short discrete heaters.

At lower values of Rayleigh number, 10^3 and 10^4 Nusselt number decreases and tends to be more uniform but still there is enhancement at the heater edges, which indicates the presence of convection even at low Rayleigh number values, Fig. 5(a). Nusselt number distribution for the opposite heating position is shown in Fig. 5(b), φ = 180º. Nusselt number is not unity at this situation, which indicates presence of convection currents, which varies between 2 and 3.7 as Rayleigh numbers increase from 10^3 to 10^6 respectively. The value of *Nu* = 1 was obtained for only fully top heated enclosures. The present results indicate clearly (φ = at 180º) that discrete heating of cavities assist the generation of flow motion (convection currents) that diminishes as the heater length increases where conduction heat transfer dominates.

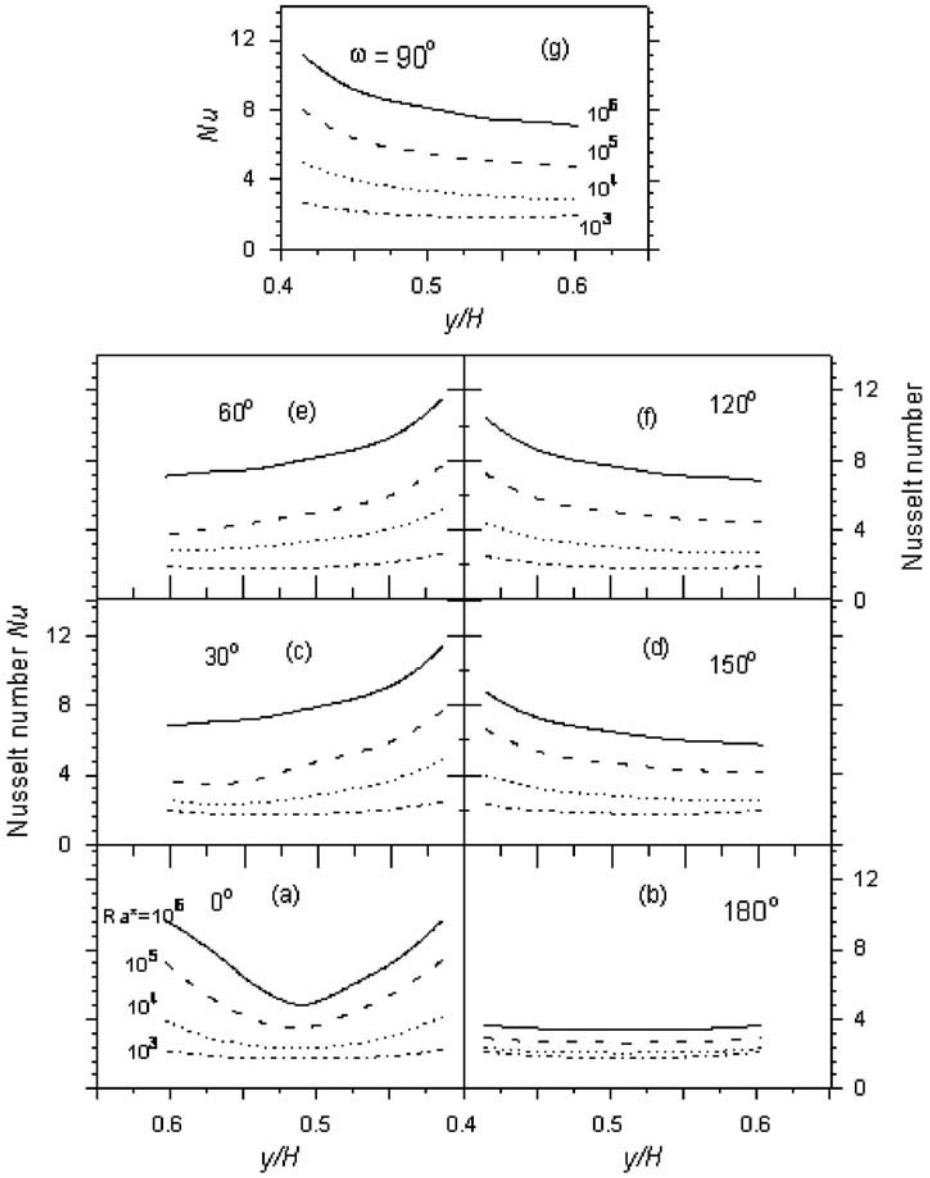

Fig. 5. Local Nusselt number variation along the heater length at tilt angles 0 to 180° and aspect ratio of 5.

At 30º angle of inclination, Fig. 5(c), Nusselt number decreases from the leading edge towards the trail of the hot section. At low Rayleigh number, this effect is not clear where Nusselt number assumes a constant value at $Nu \cong 2$ at $Ra^* = 10^3$. Similar variation is observed for $\varphi = 150º$ for which the hot surface is facing downward (Fig. 5d). The values of Nu are lower than those for the upward facing hot surface especially at $Ra^* = 10^5$ and 10^6. The streamline variations shown in Fig. 3 explain this result where at $\varphi = 30º$ the circulation cell fills the whole enclosure so that the fluid is in contact with nearly the total length of the cold surface. On the contrary, the downward facing hot surface at $\varphi = 150º$ shows a squeezed circulation cell with the tendency of the fluid to form a secondary circulation cell at the lower section of the cavity. Further rotation of the enclosure to 60º and the corresponding position at $\varphi = 120º$ give similar local Nusselt number variations as shown in Fig. 5(e and f). At the vertical position, the dependence of Nusselt number on both Ra^* and the distance y/H shows the same features where the value of Nu is the highest at the leading edge and decreases with the length in the flow direction and with the decrease of Ra^* (Fig. 5g).

The effect of the tilt angle on the average Nusselt number, $\overline{Nu}$ for fixed values or Rayleigh numbers is shown in Fig. 6. Independence on the tilt angle at low Rayleigh numbers, 10^3, with nearly fixed value of $\overline{Nu} = 2$ is observed. At higher Rayleigh number the average Nusselt number slightly decreases with the increase of the tilt angle reaching a minimum at a particular angle followed by a sharp increase to maximum before decreasing to the lowest value at $\varphi = 180º$ (top heating). The angle for the first minimum corresponds to the transition of the flow from two cells pattern to a unicellular flow.

Figure 6 indicates that this transition occurs at $\varphi \approx 15º$ for $Ra^* = 10^6$. Transition occurs at different tilt angles for different values of Rayleigh number. At $Ra^* = 10^5$ the transition occurs between 60 and 75º (Fig. 6). At the vertical position the flow is of a single cell pattern. Further increase in φ tends to develop, once again, a multiple cells pattern at φ close to 180º. This second transition is marked by change in gradients of $\overline{Nu}$ versus φ curves, Fig. 6, and for $Ra^* = 10^6$ the second transition occurs at 145º.

The observed Nusselt number dependence on the tilt angle is different from that for fully heated enclosures. The maximum Nusselt number is not obtained at the horizontal position; it is rather close to the vertical orientation. In addition, with discrete heating, there is an appreciable convection for the case of top heating that is damped as the heater length increases to approach $Nu = 1$ for fully heated enclosure. Few data points for $L/H = 1$, at $Ra = 10^6$ and $60º \leq \varphi \leq 160º$ (Ref. [14]) are plotted in the figure indicating the tendency of Nu to

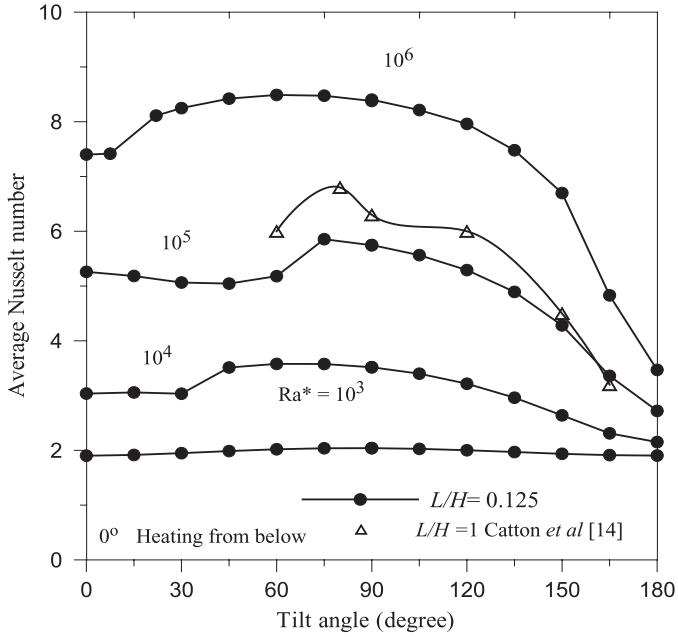

Fig. 6. Variation of average Nusselt number with tilt angle for discretely heated rectangular enclosure, Ar = 5.

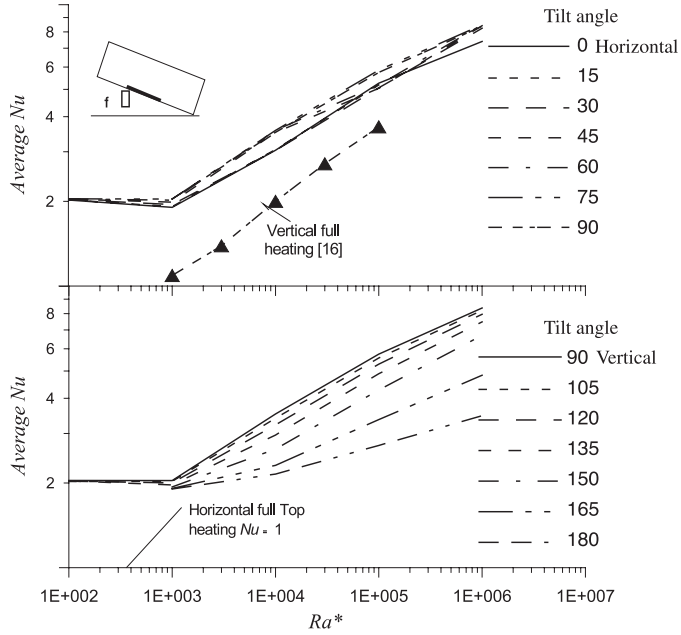

Fig. 7. Average Nusselt number variation with the modified Rayleigh number, Ar = 5.

decrease with the heater length. The present results are plotted in Fig. 7 along with Nusselt number data for the limiting cases of fully heated vertical[17] and horizontal top[21] heating correlations. Figure 7 illustrates the difference between fully and discrete heated enclosures, which is mainly caused by the differences in flow structure.

6. Conclusions

Steady natural convection in a discretely heated rectangular air-filled enclosure of aspect ratio = 5 is numerically studied for a wide range of tilt angles (from 0 to 180º) and modified Rayleigh number from 10^3 to 10^6. Streamlines and isotherms contours over the entire range of tilt angles at $Ra^* = 10^6$ are presented and discussed. At the horizontal position (heating from the bottom), the flow forms two cells pattern with a mushroom like isotherms, which is different from the case with full active hot wall. As the tilt angle increases transition from the two cells pattern to a single cell structure takes place at a certain critical angle, which depends on Rayleigh number and is associated with solution instability. At tilt angles greater than the critical one the flow is characterized by a single prolonged cell, which is squeezed towards the upper part of the enclosure at tilt angles larger than 90º (downward facing hot surface). At φ = 180º (heating from the top) the end effects of the discrete heater enhance convection, which creates circulation cells within the top section of the enclosure such that the average Nusselt number differs from unity. The variation of Nusselt number for discrete heating is different from the well-established fully heated enclosure in two aspects: a) the maximum Nusselt number is obtained at angles close to the vertical orientation. b) at the gravitationally stable condition of top heating, there is convection in the upper zone of the enclosure, while conduction is the dominating heat transfer mechanism elsewhere.

Acknowledgments

The authors would like to thank Professor S. Elsherbiny of Alexandria University for the constructive discussions and many suggestions.

Nomenclature

Ar	Aspect ratio = H/W
c_p	specific heat at constant pressure, $J.K^{-1}$. kg^{-1}
g	gravitational acceleration, m. s^{-2}
Gr	Grashof number, $g \beta \Delta T W^3/\upsilon^2$
H	enclosure height, m

k	thermal conductivity, J. m^{-1} K^{-1}
L	heater length, m
Nu	local Nusselt number, $qW/k\Delta T$
Pr	Prandtl number, $c_p\,\mu/k$
q	heat flux, W. m^{-2}
R	normalized residue
Ra	Rayleigh number, $g\,\beta\Delta T\,W^3/(\upsilon\alpha)$
Ra^*	modified Rayleigh number, $g\,\beta\,q\,W^4\,/\,(k\upsilon a)$
s	distance to the center of the heater, m
ΔT	temperature reference scale, $qW\,/\,k$, K
T	temperature, K
u, v	velocity components in the x and y directions, m. s^{-1}
U, V	dimensionless velocity components $U = uW\,/\,\upsilon$, $V = yW\,/\,\upsilon$
W	width of enclosure , m
x, y	space coordinates in Cartesian system
X, Y	dimensionless Cartesian coordinates, $X = x\,/\,W$, $Y = y\,/\,W$

Greek Symbols

α	thermal diffusivity = $k\,/\,\rho_c\,c_p$, m^2. s^{-1}
β	coefficient of volumetric thermal expansion, K^{-1}
γ	ratio of heater length to enclosure height = L/H
θ	dimensionless temperature = $k\,(T - T_c)\,/\,qW$
ε	ratio of distance to center of heater to enclosure height s/H
λ	dummy variable
μ	dynamic viscosity, kg. m^{-1} s^{-1}
υ	kinematic viscosity, m^2. s^{-1}
ρ	variable density = $\rho_c\,[1 - \beta\,(T - T_c)\,]$, kg. m^{-3}
ρ_c	density at T$_c$, kg. m^{-3}
ψ	non-dimensional stream function = $\psi_d\,/\,\nu$

τ non-dimensional time = $t\, v_o \,/\, W$

ω non-dimensional vorticity = $\omega_d\, W^2 / v_o$

Subscripts

c cold surface

d dimensional

h hot surface

Superscripts

— average value

References

[1] **Catton I.,** Natural Convection in Enclosures, *Proceedings, 6th Int. Heat Transfer Conf. Toronto, Canada*, **6:** 13-43 (1979).

[2] **Yang K., T.,** Natural Convection in Enclosures, In: **S. Kakac, R. Shah** and **W. Aung** (Eds.), *Handbook of Single-Phase Convective Heat Transfer*, Wiley, New York, Chap. 13 (1987).

[3] **Ostrach, S.,** Natural Convection in Enclosures, *ASME, J. Heat Transfer*, **110:** 1175-1190 (1988).

[4] **Khalifa, A.,** Natural Convection Heat Transfer Coefficient – a review II, Surfaces in Two- and Three- Dimensional Enclosures, *Energy Conv. Mgmt*., **42:** 505-517 (2001).

[5] **De Vahl, Davis, G.,** Natural Convection of Air in a Square Cavity: A Bench-mark Numerical Solution, *International Journal of Numerical Methods in Fluids*, **3:** 249-264 (1983).

[6] **Markatos, N.C.** and **Pericleous, K.A.,** Laminar and Turbulent Natural Convection in an Enclosure Cavity, *International Journal of Heat and Mass Transfer*, **27** (5): 755-772 (1984).

[7] **Barakos, G., Mitsoulis, E.** and **Assimacopoulos, D.,** Natural Convection Flow in a Square Cavity, Revisited; Laminar and Turbulent Models with Wall Functions, *International Journal for Numerical Methods in Fluids*, **18:** 695-719 (1994).

[8] **El-Refaee, M.M., ElSayed, M.M., Alnajem, N.M.** and **Megahid, I.E.,** Steady State Solutions of Buoyancy-Assisted Internal Flows Using a Fast False Implicit Transient Scheme (FITS), *Int. J. Num. Methods Heat Fluid Flow*, **6** (6): 3-23 (1996).

[9] **Kimura, S.** and **Bejan, A.,** The Boundary Layer Natural Convection Regime in a Rectangular Cavity with Uniform Heat Flux from the Side, *J. Heat Transfer*, **106:** 98-103 (1984).

[10] **Skouta, A., Randriazanamparanty, M.A**. and **Daguenet, M.I.,** Numerical Study of Two-Dimensional Transient Convection in an Air Filled Square Enclosure, Tilted In Relation To The Horizontal Plane, Heated from Two Opposite Sides, *International Journal of Therm. Sci*., **40:** 352-365 (2001).

[11] **Dropkin** and **Somerscales, E.,** Heat Transfer by Natural Convection in Liquids Confined by the Parallel Plates which Are Inclined at Various Angles with Respect to the Horizontal, *J. Heat Transfer*, **87:** 77-84 (1965).

[12] **Hart, J.E.,** Stability of the Flow in a Differentially Heated Inclined Box, *J. Fluid Mech*., **47:** 547-576 (1971).

[13] **Ayyaswamy, P.S.** and **Cotton I.,** The Boundary Layer Regime for Natural Convection in a Differentially Heated, Tilted Rectangular Cavity, *J. Heat Transfer*, **95:** 543-545 (1973).

[14] **Catton, I., Ayyaswamy, P.S.** and **Clever, R.M.,** Natural Convection Flow in a Finite Rectangular Slot Arbitrarily Oriented with Respect to Gravity Vector, *International Journal of Heat and Mass Transfer*, **17:** 173-184 (1974).

[15] **Ozoe, H., Yamamoto, K., Sayama, H.** and **Churchil, S.W.,** Natural Convection in an Inclined Rectangular Channel Heated on One Side and Cooled on the Opposing Side, *Int. J. Heat Mass Tran*., **17:** 1209-1217 (1974).

[16] **Elsherbiny, S.M., Raithby, G.D.** and **Hollands, K.G.T.,** Heat Transfer by Natural Convection Across Vertical and Inclined Air Layers, *J. Heat Transfer*, **104:** 96-102 (1982).

[17] **Raithby, G.D.** and **Hollands, K.G.T.,** Natural Convection, in: *Handbook of Heat Transfer Fundamentals*, **W.M. Rohsenow, J.P. Hartnett** and **E.N. Ganic** (Eds.), 2nd edition, McGraw-Hill, Chapter 6: 57-62 (1985).

[18] **Ozoe, H., Mouri, A., Omuro, M., Churchill, S.W.** and **Lior, N.,** Numerical Calculations of Laminar and Turbulent Natural Convection in Water in Rectangular Channels Heated and Cooled Isothermally on the Opposing Vertical Walls, *Int. J. Heat Mass Tran.*, **28:** 125-138 (1985).

[19] **Hamady, F.J., Lloyd, J.R., Yang, H.Q.** and **Yang, K.T.,** Study of Local Natural Convection Heat Transfer in an Inclined Enclosure, *Int. J. Heat Mass Tran.*, 9: 1697-1708 (1989).

[20] **Kuyper, R.K., Van Der Meer, T.H.H., Hoogendoorn, C.J.** and **Henkes, R.A.,** Numerical Study of Laminar and Turbulent Natural Convection in an Inclined Square Cavity, *Int. J. Heat Mass Tran*., **36:** 2899-2911 (1993).

[21] **Elsherbiny, S.M.,** Free Convection in Inclined Air Layers Heated from above, *Int. J. Heat Mass Tran.*, **39:** 3925-3930 (1996).

[22] **Incropera, F.P.,** Convection Heat Transfer in Electronic Equipment Cooling, *J. Heat Transfer*, **110:** 1097-1111 (1988).

[23] **Sathe, S.** and **Sammakia, B.,** A Review of Recent Developments in Some Practical Aspects of Air-cooled Electronic Packages, *J. Heat Transfer*, **120:** 830-838 (1998).

[24] **Teertstar, P.M., Yovanovich, M.M.** and **Culham, J.R.,** Modeling of Natural Convection in Electronic Enclosures, *IEEE Intersociety Conference on Thermal Phenomena:* 140-149 (2004).

[25] **Chu, H.H., Churchill, S.W.** and **Patterson, C.P.V.,** The Effect of Heater Size, Location, Aspect Ratio and Boundary Conditions on Two Dimensional Laminar Natural Convection in Rectangular Channel, *J. Heat Transfer*, **98:** 194-201 (1976).

[26] **Refai, G.** and **Yovanovich, M.M.,** Numerical Study from Discrete Heat Sources in a Vertical Square Enclosure, *AIAA, 28th Aerospace Science Meeting, Reno NV*, Paper No. 90-0256 (1991).

[27] **Refai, G.** and **Yovanovich, M.M.,** Influence of Discrete Heat Source Location on Natural Convection Heat Transfer in a Vertical Enclosure, *J. Electronic Packaging*, **113:** 268-274 (1991).

[28] **Chadwick, M.L., Webb, B.W.** and **Heaton, H.S.,** Natural Convection from Two-Dimensional Discrete Heat Sources in a Rectangular Enclosure, *Int. J. Heat Mass Tran.*, **34:** 1679-1693 (1991).

[29] **Turner, B.L.** and **Flack, R.D.,** The Experimental Measurement of Natural Convective Heat Transfer in Rectangular Enclosure with Concentrated Energy Sources, *J. Heat Transfer*, **102:** 236-241 (1980).

[30] **Ho, C.J.** and **Chang, J.Y.,** A Study of Natural Convection Heat Transfer in a Vertical Rectangular Enclosure with Two-Dimensional Heating: Effect of Aspect Ratio, *Int. J. Heat Mass Tran*., **37:** 917-925 (1994).

[31] **Keyhani, M., Prasad V.** and **Cox, R.,** An Experimental Study of Natural Convection in a Vertical Cavity with Discrete Heat Sources, *J. Heat Transfer*, **110:** 616-624 (1988).

[32] **Radhwan, A.** and **Zaki, G.M.,** Laminar Convection in a Square Enclosure with Discrete Heating of Vertical Walls, *J. Engineering Science, King Abdulaziz University, Jeddah, Saudi Arabia*, **12:** 70-77 (1999).

[33] **Al-Bahi A., Radhwan A.** and **Zaki G. M.,** Laminar Natural Convection from an Isoflux Discrete Heater in a Vertical Cavity, *Arab J. Sci. Eng*., **27:** 20-29 (2002).

[34] **Da Silva, A.K., Lorente, S.** and **Bejan, A.,** Optimal Distribution of Discrete Heat Sources on a Wall with Natural Convection, *Int. J. Heat Mass Trans*., **47:** 203-214 (2004).

[35] **Deng, Q., Tang, G.** and **Li, Y.,** A Combined Temperature Scale for Analyzing Natural Convection in Rectangular Enclosures with Discrete Wall Heat Sources, *Int. J. Heat Mass Trans*., **45:** 3437-3446 (2002).

[36] **Tou, S.K.W.** and **Zhang, X.F.,** Three-Dimensional Numerical Simulation of Natural Convection in an Inclined Liquid-Filled Enclosure with an array of Discrete Heaters, *Int. J. Heat Mass Tran*., **46:** 127-138 (2003).

[37] **Sezai, I.** and **Mohamad, A.A.,** Natural Convection from a Discrete Heat Source on the Bottom of a Horizontal Enclosure, *Int. J. Heat Mass Tran.*, **43:** 2257-2266 (2000).

[38] **Nogotov, E.F.,** *Applications of Numerical Heat Transfer*, McGraw-Hill, NY, pp: 00-109 (1976).

[39] **Al-Bahi, A.M.** and **Abdelrahman, M.M.,** On the Solution of Unsteady Viscous Incompressible Flow Problems, *J. AIAA*, **96:** 0826 (1996).

[40] **Shyy, W., Thakur, S.** and **Wright, J.,** Second-Order Upwind and Central Difference Schemes for Recalculating Flow Computation, *J. AIAA*, **30:** 923-932 (1992).

انتقال الحرارة بالحمل الحر داخل وعاء مستطيل المقطع من مصدر تسخين محدود الأبعاد

على الباهى* ، و ماجد الحازمى ، و جلال زكى**

** قسم الهندسة الميكانيكية و ** قسم هندسة الطيران ،كلية الهندسة*
جامعة الملك عبد العزيز ، جـــدة – المملكة العربية السعودية

المستخلص. الدراسة خاصة بانتقال الحرارة بالحمل الحراري الحر داخل وعاء مستطيل المقطع بواسطة سخان محدود الأبعاد (ارتفاع / طول الضلع = ١٢٥ , ٠) مثبت على أحد الأوجه بينما السطح المقابل عند درجة حرارة منخفضة وثابتة. تم حل معادلات بقاء الطاقة والحركة والكتلة في إتجاهين في حالة التغير مع الزمن بالطرق العددية وذلك عند زوايا ميل تتغير بين صفر و ١٨٠ درجة مع الأفقى. أوضحت النتائج أن رقم نوسلت المحلي تنخفض قيمته كلما زادت المسافة من حافة السخان عند ثبات رقم رالى ، وكذلك إعتماد كل من خطوط درجة الحرارة الثابته والتدفق على زاوية الميل ولقد تم توضيح تغير كل من رقم نوسلت ورالى وزاوية الميل . الدراسة تغطي المدى لرقم رالى من $(١٠)^{٣}$ إلى $(١٠)^{٦}$.